Plasma-catalytic ammonia synthesis in a dielectric barrier discharge reactor

A combined experimental study and kinetic modeling

Andersen, J. A.; Holm, M. C.; van 't Veer, K.; Christensen, J. M.; Østberg, M.; Bogaerts, A.; Jensen, A. D.

Published in:
Chemical Engineering Journal

Link to article, DOI:
10.1016/j.cej.2023.141294

Publication date:
2023

Document Version
Publisher's PDF, also known as Version of record

Chemical Engineering Journal 457 (2023) 141294

Contents lists available at ScienceDirect

Chemical Engineering Journal

journal homepage: www.elsevier.com/locate/cej

Plasma-catalytic ammonia synthesis in a dielectric barrier discharge reactor: A combined experimental study and kinetic modeling

J.A. Andersen [a], M.C. Holm [a], K. van 't Veer [b], J.M. Christensen [a], M. Østberg [c], A. Bogaerts [b], A.D. Jensen [a,*]

[a] Department of Chemical and Biochemical Engineering, Technical University of Denmark, 2800 Kgs. Lyngby, Denmark
[b] Research Group PLASMANT, Department of Chemistry, University of Antwerp, 2610 Wilrijk, Belgium
[c] Topsoe A/S, Haldor Topsøes Allé 1, 2800 Kgs. Lyngby, Denmark

ARTICLE INFO

Keywords:
Ammonia Synthesis
Plasma Catalysis
DBD Plasma
Chemical Kinetics Model
Micro-Discharges

ABSTRACT

Plasma-catalytic ammonia synthesis in a dielectric barrier discharge reactor has emerged as a possible route for electrification of nitrogen fixation. In this study, we use a combination of experiments and a plasma kinetic model to investigate the ammonia synthesis from N_2 and H_2, both with and without a solid packing material in the plasma zone. The effect of plasma power, feed flow rate, N_2:H_2 feed ratio, gas residence time, temperature, and packing material ($MgAl_2O_4$ alone or impregnated with Co or Ru) on the ammonia synthesis rate were examined in the experiments. The kinetic model was employed to improve our understanding of the ammonia formation pathways and identify possible changes in these pathways when altering the N_2:H_2 feed ratio. A higher NH_3 synthesis rate was achieved when increasing the feed flow rate, as well as when increasing the gas temperature from 100 to 200 °C when a packing material was present in the plasma. At the elevated temperature of 200 °C, an optimum in the NH_3 synthesis rate was observed at an equimolar feed ratio (N_2:H_2 = 1:1) for the plasma alone and $MgAl_2O_4$, while a N_2-rich feed was favored for Ru/$MgAl_2O_4$ and Co/$MgAl_2O_4$. The optimum in the synthesis rate with the N_2-rich feed, where high energy electrons are more likely to collide with N_2, suggests that the rate-limiting step is the dissociation of N_2 in the gas phase. This is supported by the kinetic model when packing material was used. However, for the plasma alone, the model found that the N_2 dissociation is only rate limiting in H_2-rich feeds, whereas the limited access to H in N_2-rich feeds makes the hydrogenation of N species limiting.

1. Introduction

A global incentive to electrify chemical processes has recently increased the interest in plasma catalysis [1–3]. This technology has shown a potential for energy storage applications such as CO_2 and CH_4 conversion [4–7], H_2 formation from NH_3 decomposition [8–11], and decentralized NH_3 synthesis [12–15]. Especially, NH_3 synthesis in dielectric barrier discharges (DBDs) has been investigated in the recent literature [16–28]. Here, a variety of potential catalytic packing materials have been examined, including γ-Al_2O_3, SiO_2, Ru/γ-Al_2O_3, Ru-Mg/γ-Al_2O_3, Ru-Cs/Si-MCM-41, Ni/SiO_2, lead zirconium titanate (PZT), and $BaTiO_3$, in various forms (powder/pellets) and sizes, which have all exhibited a beneficial effect in plasma-catalytic NH_3 synthesis. The introduction of solids in the plasma increases the complexity of the process and affects the discharge characteristics and reaction kinetics [29]. However, many of these materials have thus far been selected without bearing in mind the specific requirements for the plasma environment [2]. Based on microkinetic modeling, Mehta et al. [30] provided some guidance in the catalyst selection process. They showed that the plasma environment shifts the optimal nitrogen bond strength, compared to thermal catalysis, as the vibrationally excited N_2 allow metals that bind N relatively weakly to achieve higher activity. Under these conditions, Co step sites were predicted to achieve the highest activity for the hydrogenation reactions leading to NH_3 [30]. Rouwenhorst et al. [16] similarly reported that vibrational excitation of N_2 in the plasma helped to overcome the dissociative adsorption energy barrier and that the following hydrogenation to NH_3 occurs mainly on the surface. However, in more recent publications by Rouwenhorst et al. [15,17], it was reported that the formation of N radicals enhanced the NH_3 synthesis when operating the plasma at elevated temperatures

* Corresponding author.
E-mail address: aj@kt.dtu.dk (A.D. Jensen).

https://doi.org/10.1016/j.cej.2023.141294
Received 18 October 2022; Received in revised form 29 December 2022; Accepted 2 January 2023
Available online 5 January 2023

(>300 °C). Engelmann et al. [18] similarly found from microkinetic modeling that the NH_3 synthesis was enhanced in a plasma with high radical densities, compared to a plasma with only vibrational excitations. It was further reported that the conditions giving the high radical densities were closer to the regime of a DBD plasma, where radical adsorptions on the surface and Eley − Rideal (ER) reactions dominate the NH_3 synthesis [18]. Based on experimental observations of similar NH_3 concentrations obtained when using different transition metal catalysts (Fe, Ru, Co, and Cu), Gorbanev et al. [19] suggested a major importance of radical adsorption and ER reactions in plasma-catalytic NH_3 synthesis, rather than dissociative adsorption of vibrationally excited molecules. A good agreement between their experimental results [19] and the computational findings of Engelmann et al. [18] was reported.

Iwamoto et al. [20] proposed that adsorption of electronically excited N_2 leads to the formation of NH_3 through reaction with surface-bound hydrogen (i.e. H(s)). Peng et al. [21] stated that NH_3 is predominantly formed through NH formed in the gas phase, which then adsorb on the surface and undergo further hydrogenation. From analysis of optical emission spectra, Gómez-Ramírez et al. [22] identified N_2^+ as the likely reaction-initiating species, which is in agreement with the experimental observations made by Bai et al. [23].

In a kinetic analysis by Hong et al. [31] it was established that the NH_3 formation initially was from interaction between surface-adsorbed NH (i.e. NH(s)) and H_2 and three-body reactions with NH, N_2 and H_2 in the gas phase. In their model, the plasma was described as a continuous low electron energy discharge. The generation of NH was found to be through reaction between N and $H_2(v)$, which both are produced by reactions involving collisions with electrons. Subsequently, the importance of surface reactions was found to increase as the discharge continued with H(s) driving the chemistry, as the formation rate of H(s) was 4 orders of magnitude higher than for surface-adsorbed N (i.e., N (s)). These surface species were largely formed by dissociative adsorption of their ground state. Furthermore, with the increasing importance of the surface reactions, the NH_3 formation was predicted to come mainly from an ER reaction between NH_2 and H(s) [31].

van 't Veer et al. [32] utilized a kinetic model to capture the role of the micro-discharges and their afterglows. They found that some of the synthesized NH_3 was decomposed during the micro-discharges. However, due to formed N and H atoms from electron impact dissociation, a net production of NH_3 in the successive afterglows was predicted through surface reactions. Significant importance of H(s) was reported, in agreement with Hong et al. [31], since the formation of NH(s) was predicted to originate from an ER reaction with N. Subsequently, NH(s) is hydrogenated to NH_3 through Langmuir − Hinshelwood (LH) reaction steps. Thereby, the rate-limiting step under the plasma-catalytic conditions was identified to be N_2 dissociation to N in the gas phase by electron impact, followed by adsorption of N on the surface.

As evident from the above discussion of the previous studies, varying reaction steps are suggested to be significant in the synthesis of NH_3 and it remains unclear which step is rate limiting. Studies that combine experiments with a kinetic analysis by modeling have the opportunity to yield a better understanding of the underlying mechanisms. Yet, many of the currently available studies are either experimental or model-based.

Therefore, a combined study of experiments and modeling work is presented in this paper. A DBD reactor was used in the experimental part where the influence of plasma power, feed flow rate, N_2:H_2 feed ratio, gas residence time, temperature, and packing material were examined. Additionally, a zero-dimensional (0D) plasma kinetic model was used to analyze the reaction kinetics and understand the performance of the individual phenomena in the plasma (micro-discharges and their afterglows).

2. Experimental

2.1. Dielectric barrier discharge setup

The experimental work was conducted using a quartz DBD reactor (outer and inner diameter of 22 and 19 mm, respectively) in a setup previously [8] described in detail. A stainless steel rod (ø: 10 mm) was used as the inner electrode, while a steel mesh of variable length (1–5 cm) was tightly wrapped around the reactor as the outer electrode. A discharge gap of 4.5 mm between the inner electrode and the reactor wall was therefore used. The outer electrode was powered by a TREK high voltage amplifier (model 20/20C-HS) controlled by a Tektronix function generator (AFG1022). To measure the current, applied voltage, and generated charges, a Rogowski coil (Pearson, 4100), a high voltage probe (Tektronix, P6015A), and a low voltage probe (Picotech, TA150) with an external capacitor (10 nF) were used, respectively. Continuous recording of current, voltage, and charges, and calculation of plasma power was done by a digital oscilloscope (Picotech, Picoscope 6402C).

The NH_3 synthesis was investigated at different plasma power (10–30 W) at a sinusoidal frequency of 3.0 kHz, apart from experiments using $Co/MgAl_2O_4$. Here a plasma power of 25 W could at maximum be attained due to limitations of the high voltage amplifier. For experiments using a packing material, the full discharge volume was filled with packing material, with glass wool placed on each side of the bed. The variable length of the outer electrode was used to modify the gas residence time, instead of altering the feed flow rate, such that a constant plasma power to feed flow rate ratio could be kept.

To investigate the effect of an increase in gas temperature, woven ceramic fibers (insulation material) were wrapped around the reactor to utilize the heat released from the plasma. The temperature was measured on the outside of the reactor wall with a thermocouple, just after the plasma was turned off, to estimate the working temperature of the reactor. Without insulation, a reactor temperature of 100 °C was consistently measured with or without the various types of packing material. When insulation was added, the thermocouple was inserted between the insulation material and the reactor wall, resulting in temperature measurements of 200–210 °C for the plasma alone and the tested packing materials. The reactor wall temperature was then assumed to be equal to the gas temperature.

Bronkhorst mass flow controllers were used to feed N_2 (99.999 % purity) and H_2 (99.999 % purity) mixtures to the reactor at flow rates of 40–100 Nml/min. Any oxygen present in the reactor was initially removed by passing a flow of N_2 through the reactor for 10 min, after which the feed ratio was applied and kept for an additional 10 min, before igniting the plasma. A period of 1 h was used to stabilize the plasma after ignition, followed by a 15 min steady state period where the concentration of NH_3 in the effluent was analyzed using an online NH_3-analyser (ABB, AO2000-Limas 11 HW gas analyzer).

2.2. Plasma-catalytic material

The effect of implementing $MgAl_2O_4$ (Topsoe A/S) or $MgAl_2O_4$ impregnated with Co or Ru in the discharge zone was investigated. Physicochemical properties of $MgAl_2O_4$ have been described in our previous work [8]. These materials were prepared by incipient wetness impregnation, using nitrate salts as the metal precursors, of $MgAl_2O_4$ pellets, after which the samples were dried and calcined at 450 °C. The pellets were then crushed and sieved to a particle size of 0.85–1.18 mm. The resulting metal-containing materials used were 2 wt% $Ru/MgAl_2O_4$ and 10 wt% $Co/MgAl_2O_4$.

Pre-reduction of the Co and Ru containing materials was done prior to use, in H_2 (300 Nl/min) at 525 °C for 8 h in a muffle furnace, followed by passivation at room temperature with 1 % O_2 in N_2. The samples were then transferred to the plasma reactor where they were re-reduced *in situ* in a 20 vol% H_2/Ar plasma (25 W at 3 kHz) with a total flow rate of 75 Nml/min for 2 h.

3. Computational method

The 0D plasma kinetics model ZDPlasKin [33,34] was used to gain insight in the effect of the N_2:H_2 feed ratio on the chemistry of the plasma-catalytic synthesis of NH_3 in a DBD reactor. The model predicts the time evolution of the species included in the kinetic model based on calculated reaction rates. These reaction rates were determined from reaction specific rate coefficients taken from an earlier version of the model [35]. The reactions incorporated in the model include collisions between electrons and heavy particles, giving rise to ionization, excitation, and dissociation, as well as reactions between heavy particles, surface adsorption, etc. A full list of the considered surface and gas phase species and chemical reactions was reported by van 't Veer et al. [35].

The base model was expanded by van 't Veer et al. [35] to include the separate behavior of the micro-discharges and their afterglows, with a power density distribution factor (γ) determining the minimum power density of the afterglow based on the maximum power density in a micro-discharge. The method to determine γ was based on the appearance of the experimental power profile, such that an agreement between the experimental and model power of the micro-discharges and the uniform plasma was achieved. This method was described in greater detail in our previous work [9]. The afterglow is a weaker and long-lasting plasma, compared to the short-lived micro-discharges (life-time ca. 100 ns) in the DBD plasma. The effect of these two plasma phenomena will also be investigated in this study. The plasma conditions used in the model to describe the micro-discharges and their afterglows were determined from the experimentally measured current, voltage, and charges. The parameters determined from the current were the number of micro-discharges per half cycle (N_{MD}) and their lifetime (τ_{MD}). From the voltage and charge measurements, the charge transfer (Q_0), burning voltage (ΔU), capacitance of the cell (C_{cell}), effective capacitance (ζ_{diel}), and dielectric capacitance (C_{diel}) were determined. Each of the fed gas mixtures yield different effects on the measured electrical parameters. These parameters were used to determine the electric field (E) and electron conductivity (σ) (see Supporting Information, section 1). A table of the obtained case-specific parameters is also shown in the Supporting Information (see Table S1).

As described in the previous work by van 't Veer et al. [32], a number of assumptions were made in the calculations of the surface kinetics, when the model was used to describe reactions in the presence of a solid packing material. One assumption concerns the value of the sticking coefficients of the gas phase species on the metal surface, which dictates the adsorption of N, H, and NH_x, thereby influencing the rate of the elementary ER and LH reactions. The coefficients used are for an iron surface, not distinguishing between steps and planar sites, as this was reported to be the most complete data set available. However, in this study no iron-based catalyst was tested. This was mainly due to the observation in our previous work [8], where iron-based catalysts were found to be difficult to reduce under the plasma conditions, causing an uncertainty about the presence of oxidized phases. Consequently, the results obtained from the model in the simulations with packing can mainly be used to qualitatively understand which additional reaction pathways a surface may provide. Further work is required for more quantitative insights.

To adapt the rate coefficients of the surface reactions from s^{-1} to cm^3 s^{-1} or cm^6 s^{-1}, a reactor specific volume-to-surface area ratio was needed. The specific surface area was determined as the sum of the electrode, reactor wall, and only the outer surface area of the particles, due to the negligible plasma propagation into the $MgAl_2O_4$ pores [36,37]. Indeed, the pore size of our catalysts is in the nm-range, which is much smaller than the Debye length at the conditions under study, and thus, too small for the plasma streamers to propagate inside the pores, as predicted by modeling [36,37]. An equal combination of spheres and cylinders was assumed as the shape of the particles, with radius and height obtained from the sieve size, which allowed for the determination of the outer surface area of particles. For the utilized reactor, this ratio was found to be 0.225 cm when no packing material was used and 0.0157 cm with packing material. Furthermore, a surface site density of 10^{15} cm^{-2} was assumed, based on a nonspecific metal surface representation [38].

In the model, the micro-discharges were assumed to be uniformly distributed in the plasma volume and to occur one at a time with a fixed time interval. However, the experimental current measurements showed that the micro-discharges mainly occur in the periods where the voltage changes from a value of zero to its maximum or minimum value (see Fig. S1). Nevertheless, a single molecule in the DBD reactor cannot interact with all the formed micro-discharges due to their short lifetime compared to the residence time of the gas (equal to the simulation time). Therefore, a probability factor was introduced, as the ratio between the time of a full discharge period and the residence time of the gas, which in turn defined how many micro-discharges a molecule encounters. Moreover, when no packing material was placed in the plasma, the volume of a micro-discharge was represented as a cylinder with the gap size (4.5 mm) as the length and the radius of the discharge equal to 0.1 mm [39]. With packing material in the plasma zone, the micro-discharge volume was represented as a sphere between solid particles. Additionally, a packing factor of 0.65 was determined for $MgAl_2O_4$, by determining the volume of water displaced by the solid material, to define the volume of gas in the reactor when packing material was included. This factor was expected to apply for the other materials as well, since $MgAl_2O_4$ was the majority component in all samples.

4. Results and discussion

4.1. Effect of plasma power on the NH_3 concentration

The influence of plasma power on the production of NH_3 is shown in Fig. 1. It can be seen that the NH_3 concentration increases with plasma power. A clear increase in the NH_3 concentration is also seen when introducing a packing material in the plasma. At a plasma power of 25 W, the presence of $MgAl_2O_4$ approximately doubles the formation of NH_3 compared to the plasma alone, while Ru/$MgAl_2O_4$ and Co/$MgAl_2O_4$ increases the formation by a factor of ca. 3 and 4, respectively. Remarkably, the NH_3 concentration achieved with the Co-catalyst at 10 W (3000 ppm) is 67 % higher than for the plasma alone at 30 W (1800 ppm). Furthermore, the NH_3 concentration reaches a plateau for the plasma alone, while a linear increasing trend is observed for the Co/$MgAl_2O_4$ packing in the tested plasma power range. The full set of data for NH_3 concentration for the plasma alone, $MgAl_2O_4$, Ru/$MgAl_2O_4$, and Co/$MgAl_2O_4$ packing, for the feed ratio range investigated (N_2:H_2 = 3:1 to 1:3) as function of plasma power is shown in the Supporting Information (see Fig. S2).

Plasma streamers are not expected to enter the pores of the packing material due to the far greater Debye length of a micro-discharge in a DBD plasma (in the order of μm) compared to the pore size of $MgAl_2O_4$ (in the order of nm) [8,36,37]. The internal porosity/surface of the plasma-catalytic material is therefore mainly expected to facilitate molecular and surface collisions and adsorb species with a sufficient lifetime to diffuse through the pore. The internal surface is therefore expected to operate as a thermal catalyst, which, under the applied conditions, most likely will have essentially zero activity.

4.2. Effect of flow rate on the NH_3 synthesis rate

Fig. 2 depicts the NH_3 synthesis rate as function of the feed flow rate with and without the insulation material. The synthesis rate is observed to increase for both the plasma alone and for the tested packing materials with increasing feed flow rate. An increase of 1.75 μmol NH_3/min (49 %) is found for the plasma alone, while the packing materials ($MgAl_2O_4$, Ru/$MgAl_2O_4$, and Co/$MgAl_2O_4$) show an increase of ca. 3 μmol NH_3/min (38 %, 23 %, and 22 %), when changing the feed flow rate from 40 to 100 Nml/min. In contrast to the NH_3 synthesis rate, the

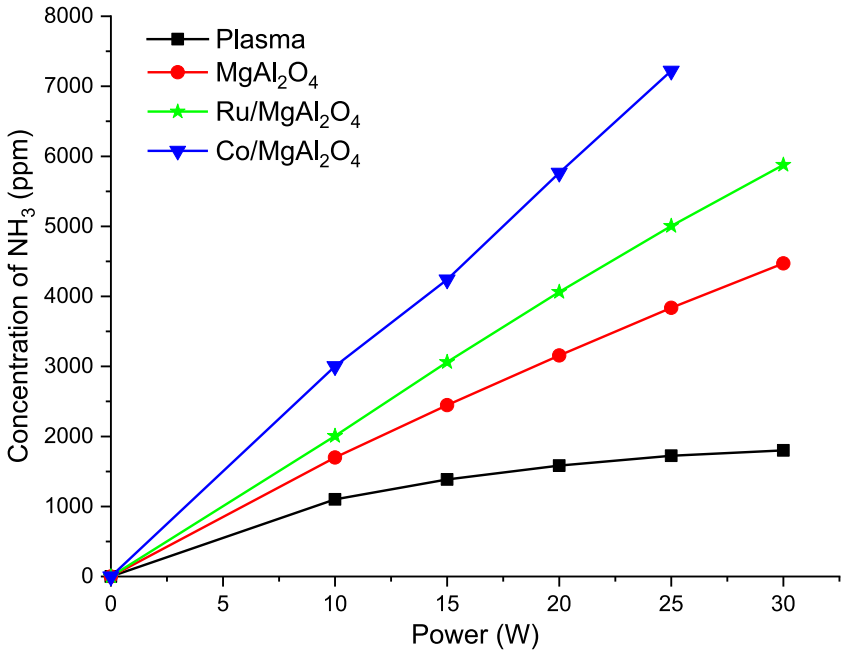

Fig. 1. NH_3 concentration as function of plasma power for different packing materials and plasma alone (Flow rate of 80 Nml/min and N_2:H_2 = 1:1).

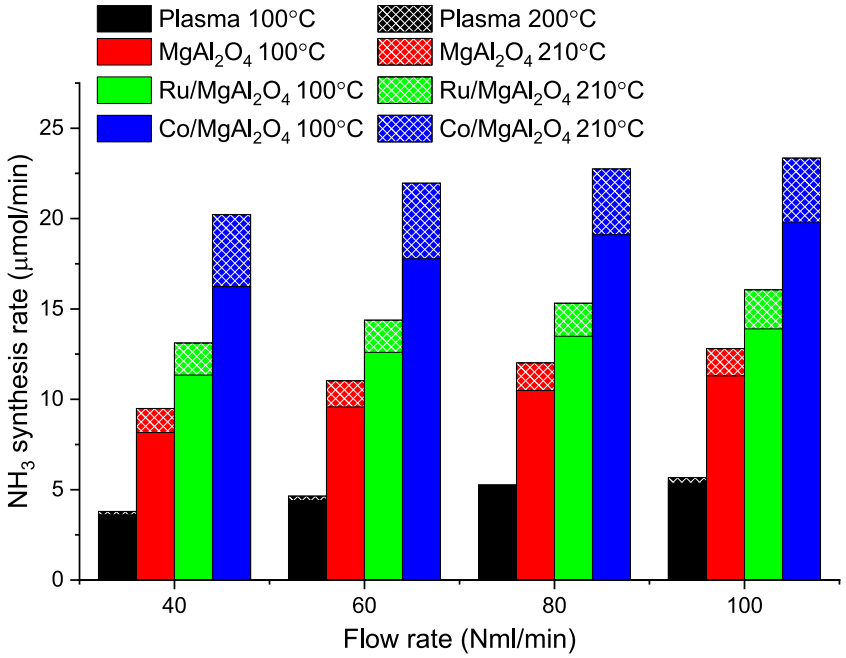

Fig. 2. Effect of the feed flow rate on NH_3 synthesis rate (plasma power 20 W at 3.0 kHz and N_2:H_2 = 1:1).

measured NH_3 concentration decreases upon increasing flow rate (see Fig. S3). It has been reported that the shorter residence time, which follows with the increase in feed flow rate, lowers the possibility of effective collisions between reactive species, thereby lowering the formation of NH_3 [23,24]. The NH_3 formation and removal rates will be discussed further below.

In our previous work [8] we reported that the plasma-catalytic NH_3 decomposition was affected negatively by a higher gas temperature (at a fixed molar feed rate), mainly due to the reduced residence time originating from the gas expansion. For the NH_3 synthesis, the effect of increasing the temperature is observed to improve the synthesis rate when packing material is utilized (patterned bars), despite the lower residence time. For the plasma alone, the change in residence time and the positive effect of the temperature increase might cancel out, as the observed reaction rate is temperature-independent. The rate increase shown by the packing materials (15–20 %) is independent of the flow rate, with the temperature affecting the synthesis rate for $Co/MgAl_2O_4$ to a larger extent, reaching a synthesis rate of 23.3 μmol NH_3/min at 100 Nml/min and 210 °C. The energy efficiency of NH_3 synthesis for the investigated conditions is shown in the Supporting Information (Figs. S4 and S5).

The temperature change is found to marginally affect the measured electrical parameters for the $Co/MgAl_2O_4$ catalyst (as illustrated for the Q-U Lissajous plot in Fig. S6), hence the increase in the synthesis rate is deemed to be due to improved reaction kinetics in the gas phase and on the surface at the elevated temperature. The plasma kinetic model

confirmed this (see Fig. S7), as increasing the gas temperature, at which the surface reactions also are evaluated, is found to result in a higher NH_3 concentration. Interestingly, the rise found by the model is 20 %, which matches that found from the experimental results.

4.3. Effect of feed ratio on the NH_3 synthesis rate

The influence of the N_2:H_2 feed ratio on the synthesis of NH_3 has been reported in previous studies [20–24,26–28], and is also investigated here. Fig. 3 shows that at 100 °C the highest NH_3 synthesis rates are achieved at an equimolar feed ratio (N_2:H_2 = 1:1) for the plasma alone, $MgAl_2O_4$, and Co/$MgAl_2O_4$ packing. Only the Ru/$MgAl_2O_4$ catalyst shows a slightly higher synthesis rate in a N_2-rich environment (N_2:H_2 = 2:1), which is similar to the findings of Kim et al. [26]. For the Ru/$MgAl_2O_4$ and Co/$MgAl_2O_4$ catalysts, the negative effect of a H_2-rich feed is found to be greater than for the plasma alone and $MgAl_2O_4$ packing, as the synthesis rate drops below that of the N_2-rich feed.

Similar to the results of the flow rate experiments, increasing the gas temperature improves the NH_3 synthesis rate at the different feed ratios when packing materials are used. However, a larger impact of increasing the temperature (from 100 to 200 °C) is observed for the N_2-rich feed, as observed in Fig. 3. For the plasma alone, a slight decrease in the NH_3 synthesis rate, too small to be visible in Fig. 3, occurs, while an increase from 19.0 to 24.6 μmol NH_3/min is found for the Co/$MgAl_2O_4$ catalyst at N_2:H_2 = 2:1, which at the elevated temperature becomes the optimal feed ratio. Having a higher content of N_2 in the feed increases the probability of N_2 dissociation, resulting in higher concentrations of N. The improved NH_3 synthesis rate at the N_2-rich feed therefore indicates that the rate-limiting step is the dissociation of N_2. This is in agreement with the findings of van 't Veer et al. [32].

Mehta et al. [30] predicted that vibrational excitation of N_2 plays an important role in the formation of N(s) when using a Co-containing catalyst. From the results in Fig. 3, it is difficult to say if the Co surface sites promote the dissociation of ground state, vibrationally exited, or electronically excited N_2 or simply increase the mobility of the surface species to promote a LH route. In contrast, van 't Veer et al. [32] did not find dissociative adsorption of vibrational/electronically excited N_2 to be of importance. Similarly, Engelmann et al. [18] reported that the contribution of catalytic dissociation of vibrationally excited N_2 towards the synthesis of NH_3 is several orders of magnitude (10^6-10^{10}) lower than from radical adsorption (ER) reactions. Hence, the vibrationally/electronically excited N_2 species might not be of great importance at the tested conditions.

Additionally, it was reported in our previous work [8] that Co/$MgAl_2O_4$ show a very low activity for plasma-catalytic NH_3 decomposition compared to the pure support material. A lower current spike intensity is observed for the Co/$MgAl_2O_4$ compared to the bare support (see Fig. S1), which is likely due to enhanced surface discharges in the presence of metal particles. This leads to weaker micro-discharges where a lower rate of NH_3 decomposition potentially occur, yielding the overall higher synthesis rate of NH_3.

The kinetic model predicts a small influence of the feed ratio on the NH_3 synthesis rate for the plasma alone (unpacked) as seen in Fig. 4. The NH_3 synthesis rate was calculated from the last determined NH_3 density by the model, which was at maximum residence time, always corresponding to the end of an afterglow. In Fig. 4, the synthesis rate is predicted to have a stable value of ca. 0.23 μmol NH_3/min for the feed ratios N_2:H_2 = 3:1 to 1:1, while the rate decreases slightly for the H_2-rich feed (0.16 μmol NH_3/min). A substantial influence of the feed ratio is predicted for the packed bed, as Fig. 4 shows a continuous decrease in reaction rate from a N_2-rich feed to a H_2-rich feed. At the feed ratio N_2:H_2 = 1:3, the synthesis rate has decreased by a factor of 3.5 relative to the value at N_2:H_2 = 3:1. The synthesis rates predicted by the model are lower than the experimental values, i.e., 17–27 times for the unpacked case and 10–28 times for the packed bed, but the qualitative trends are described well by the model. Both the several fold increase in the rate due to a metal-containing packing material and the difference between a N_2:H_2-ratio dependent rate with the packing material and the ratio-independent rate for plasma alone are described well by the model. The model's ability to describe the qualitative behavior suggests that the model captures the important trends in the underlying mechanism of NH_3 synthesis. The differences in absolute rates are most likely a result of assumptions made in the model, interpretation and translation of experimental electrical data (N_{MD}, τ_{MD}, Q_0, ΔU, C_{cell}, ζ_{diel}, C_{diel}) to the model, and uncertainty in the kinetic parameters, especially with respect to the catalytic kinetics (see section 3 Computational method above, and Supporting Information). In the following sections, we will present more detailed computational results, to obtain further insights in the underlying mechanism of NH_3 synthesis.

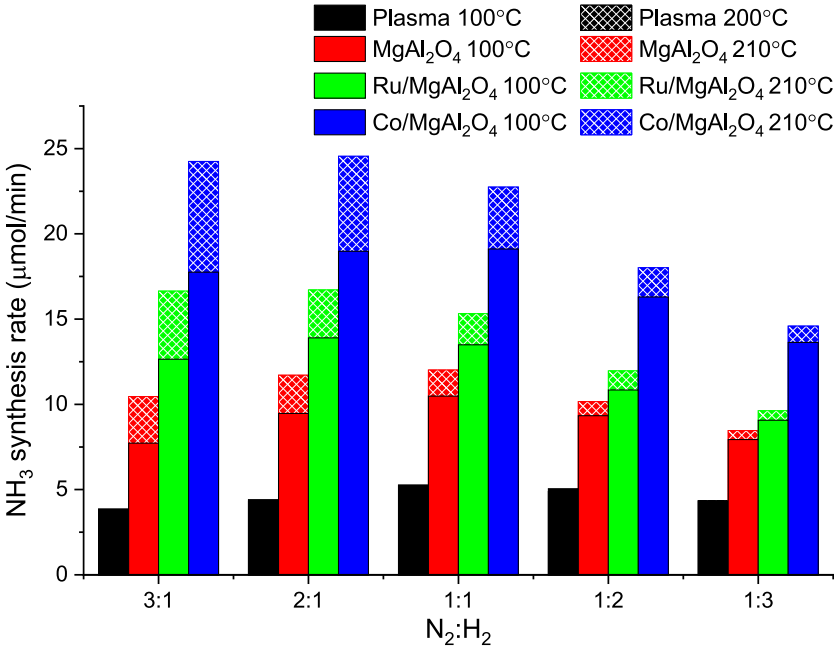

Fig. 3. Effect of N_2:H_2 feed ratio on NH_3 synthesis rate (plasma power 20 W at 3.0 kHz and flow rate of 80 Nml/min).

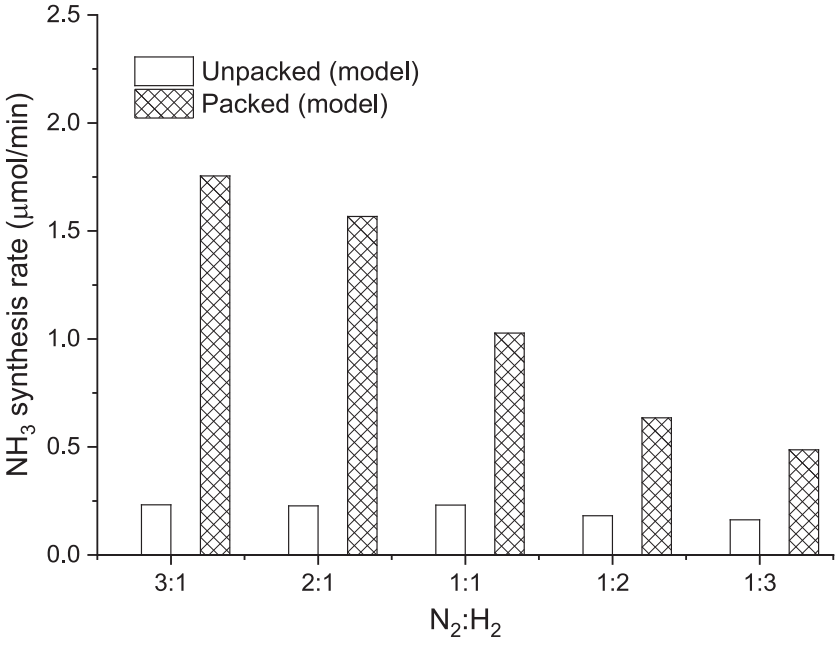

Fig. 4. Simulated effect of N_2:H_2 feed ratio on NH_3 synthesis rate. Model input parameters are shown in Table S1.

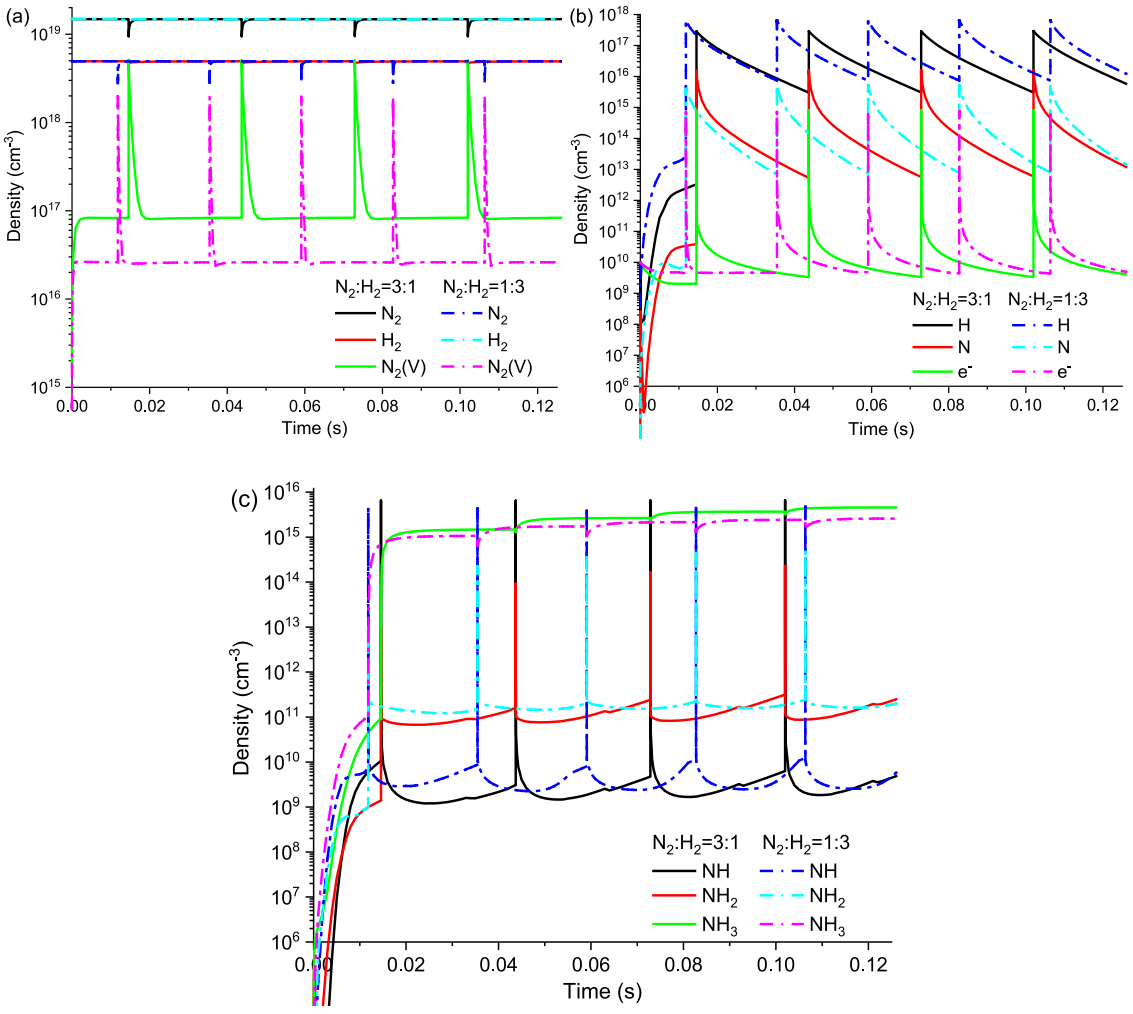

Fig. 5. Transient number density of (a) ground state and vibrationally excited molecules, (b) radicals and electrons, and (c) NH_x species, for the feed ratios N_2:H_2 = 3:1 (solid lines) and 1:3 (dashed lines). The case-specific conditions are shown in Table S1.

4.4. Transient plasma species densities and surface coverages at different feed ratios

The model predicts the time-evolution of the density (concentration) of the various species considered, i.e., ground state and excited molecules and atoms, ions, radicals, electrons, and surface adsorbed species (noted by X(s)). Fig. 5 depicts the transient progress in the concentration of selected gas phase species from the start of the plasma to a residence time of 125 ms. After the 125 ms, the system has reached a state where the densities in the next cycle (micro-discharge and afterglow) resembles the previous, except for NH_3, which continues to show a slow increase in density upon increasing residence time. In Fig. 5 we only illustrate the density of the N_2:H_2 = 3:1 and 1:3 feed ratios, as these show the biggest differences in synthesis rates (cf. Fig. 4). Within the plotted residence time, four micro-discharges are encountered for the N_2:H_2 = 3:1 feed ratio and 5 for N_2:H_2 = 1:3. The frequency of micro-discharges in the model is determined based on the experimental number of micro-discharges per half cycle (noted in Table S1).

The density of all the gas-phase species increases during the initial milliseconds, except for the feed gas species (N_2 and H_2), which also are the only species that do not show an increase in density during the micro-discharges (Fig. 5). During the micro-discharges, the densities of vibrationally excited N_2 (N_2(V)), NH, and NH_2 rise very quickly to then almost immediately drop back to more or less the same values, as soon as the strong plasma environment of the micro-discharges wears off. The density of N_2(V) in the N_2-rich feed is predicted to be ca. 3 times higher than in the H_2-rich feed, which matches the difference in N_2 density in the feed (cf. Fig. 5a). Interestingly, the density of NH is predicted to reach a higher peak value for the N_2:H_2 = 3:1 feed ratio, but with the feed ratio N_2:H_2 = 1:3 a higher NH_2 peak density is obtained (see Fig. 5c). According to the model, this is because the main formation path of NH_2 is not through NH, but from dissociation of NH_3 in the micro-discharges.

Contrary to the behavior of N_2(V), NH, and NH_2, the densities of H and N are found to decrease slowly after the micro-discharges, showing that these radicals have a longer lifetime. Additionally, it can be observed on Fig. 5b that the density of H is higher than that of N, independent of the feed ratio, which can be attributed to the lower bond strength of H_2 (4.5 eV) compared to N_2 (9.8 eV) [40]. Yet, the N_2-rich feed yields a ca. 3 times higher maximum density of N (1.56×10^{16} cm^{-3}) compared to the H_2-rich feed (5.22×10^{15} cm^{-3}), which almost correlates with the difference in NH_3 synthesis rate (factor of 3.5). Fig. 6 shows the model prediction of the NH_3 synthesis rate (see Fig. 4) for the unpacked and packed setup as a function of the maximum simulated N density across the variations in the N_2:H_2 ratio. Each data point in Fig. 6 (calculated maximum density of N and NH_3 synthesis rate) is obtained from one feed ratio and then divided by the values obtained from the feed ratio of N_2:H_2 = 3:1, thereby yielding the point of (1,1) furthest to the right.

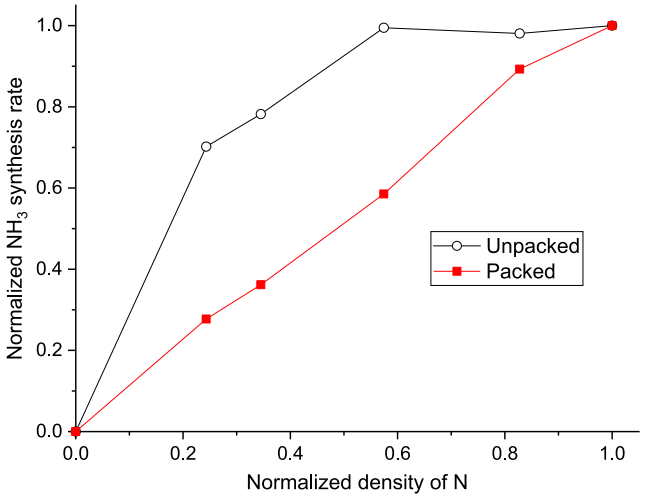

Fig. 6. Correlation between the normalized maximum density of N atoms in a micro-discharge and the normalized NH_3 synthesis rate. Both the densities and the synthesis rates are normalized with the obtained values from the feed ratio N_2:H_2 = 3:1.

Fig. 6 shows a linear relationship between the maximum density of N in the micro-discharges and the NH_3 synthesis rates in the presence of a packing material, indicating that the formation of N is the rate-limiting step for all the feed ratios (N_2:H_2 = 3:1 to 1:3) under the tested conditions, similar to the observation made from the experiments. This is also in agreement with the observation made by Navascués et al. [41], who used a surface reaction model and found that the rate-limiting step is the dissociation of N_2 in the plasma, and by Engelmann et al. [18], who found a direct relation between the plasma-catalytic NH_3 synthesis and the density of N atoms in the gas phase from microkinetic modeling. However, the mechanism is complicated and therefore a degree of rate control analysis is needed to unambiguously determine the rate-limiting step [42].

For the plasma alone, the NH_3 synthesis rate is constant when a N_2-rich feed is used (N_2:H_2 = 3:1 to 1:1, corresponding to the last three points to the right in Fig. 6). This indicates that a different set of reactions are rate-limiting at these feed ratios, which could be the hydrogenation of N atoms to NH, as the access to hydrogen is limited without the surface. The formation of NH has also been reported by Navascués et al. [41] to be a limiting reaction in the formation of NH_3.

Additional reactions are introduced when using a packing material, which shifts the sole need for collisions in the gas phase to progress the NH_3 formation, to include ER and LH reactions on the surface sites of the packing material. Similar to the gas-phase species, the adsorbed species show an increase in the surface coverage during the initial milliseconds and during the micro-discharges (except H(s)), as seen in Fig. 7. H(s) is found to be the main adsorbate independent of feed ratio, and with an almost constant coverage for the N_2:H_2 = 1:3 feed ratio. Similar results were obtained by Hong et al. [31], who found H(s) to be the main surface specie, followed by N(s). However, they found the NH_2(s) coverage to be higher than that of NH(s), which is opposite to the results shown in Fig. 7. It should be noted that the model used by Hong et al. [31] did not take into account the strong and weaker plasma characteristic for the micro-discharges and their afterglows. In view of this, their results are only expected to partly agree with our results. A closer look at the results obtained by Hong et al. [31] reveals that during the initial milliseconds the NH(s) coverage is actually higher than the NH_2(s) coverage, which is similar to Fig. 7, until the time frame where the first micro-discharge occurs.

The surface coverage of H(s) is found to decrease during the micro-discharges (change too small to be fully visible in Fig. 7) for both feed ratios, resulting in a slight increase in empty-sites. In the afterglows, the H(s) coverage increases to the same value as before the micro-discharges by re-occupation of the empty-sites. This high coverage of H(s) leads to reactions with N to form NH(s) (discussed further below). Additionally, the N_2-rich feed shows a higher peak coverage of N(s), NH(s), and NH_2(s) during the micro-discharges. The higher NH_3 synthesis rate for this feed ratio, seen in Fig. 3 and Fig. 4, can partly be explained by this observation, as these surface species previously have been identified to be more dominant in the formation of NH_3 compared to their gas phase equivalents (N, NH, and NH_2) [16,31,43].

4.5. Predicted time-averaged source terms of gas phase and adsorbed species at different feed ratios for the packed setup

To understand the difference in the synthesis rate for the packed setup due to the change in feed ratio, the time-average source term (S) for N_2, N, H_2, H, NH_x, electrons, and the surface species are presented in Fig. 8 for the two extremes in the feed ratio (N_2:H_2 = 3:1 and 1:3). As

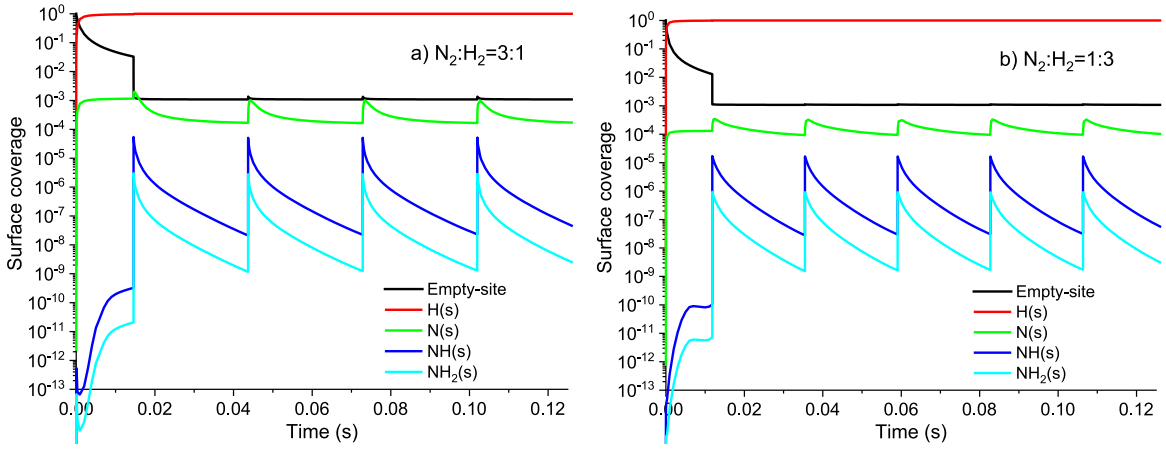

Fig. 7. Fraction of empty sites and surface species as function of residence time for a) N_2:H_2 = 3:1 and b) N_2:H_2 = 3:1. The case-specific conditions are shown in Table S1.

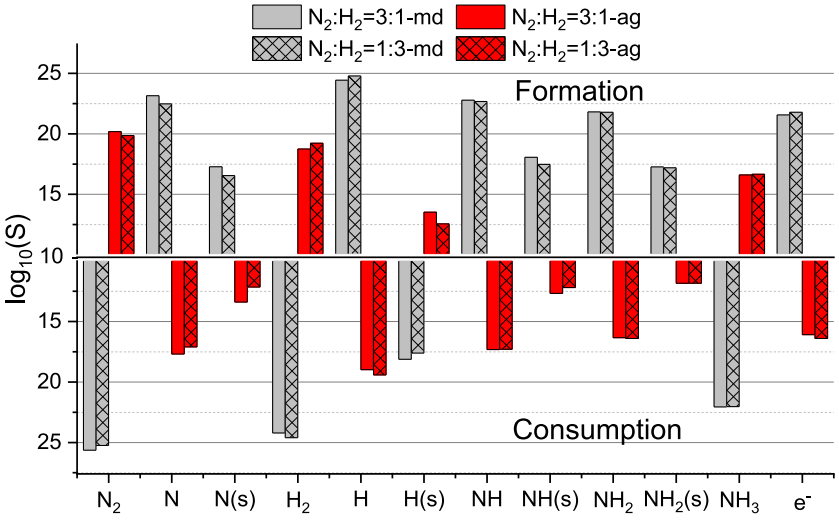

Fig. 8. Time-average source terms (S_i) ($cm^{-3}\ s^{-1}$) for neutral gas phase and surface-adsorbed species and electrons in a micro-discharge (md) and its afterglow (ag) for the packed setup.

described earlier, the dissociation of N_2 is believed to be the rate-limiting step, hence it is of great importance to form N, and possibly N (s), to yield a higher NH_3 synthesis. When comparing the consumption of N_2 and the formation of N and N(s) for the two feed ratios, it is clearly seen that the N_2-rich feed shows higher N_2 consumption and formation of N and N(s) in the micro-discharges (md, grey bars). A higher removal of N and N(s) is also observed in the afterglows (ag) for this feed ratio (red bars). On the other hand, the H_2-rich feed shows higher source terms for the removal of H_2 and the formation of H and H(s). Similar to the observation in Fig. 7, Fig. 8 shows that H(s) is consumed in the micro-discharges and formed in the afterglows, which is opposite to the other surface species. This is mainly due to the high density of H in the gas phase (see Fig. 5b), which reacts with H(s) to form again H_2 and an empty-site (Reaction 1). This ER route was also reported by Shah et al. [44] to dominate the re-formation of H_2 over the LH route.

$$(\mathrm{md})\quad \mathrm{H} + \mathrm{H(s)} \rightarrow \mathrm{H_2} + \mathrm{surf} \tag{R1}$$

As mentioned previously, the N_2-rich feed has a higher formation of NH and NH(s) compared to the H_2-rich feed. Yet, for both feed ratios, the NH formation mainly occur through collision of N and electronically excited states of H_2 (Reaction 2 to 4), which is true for both the micro-discharges (contribution of 89 %) and their afterglows (contribution of 80 % for N_2:H_2 = 3:1 and 94 % for N_2:H_2 = 1:3). However, the reaction rates strongly depend on the feed ratio, with the rate of Reaction 3 showing the highest level of dependence in the micro-discharges ($7.84 \times 10^{21} \rightarrow 1.02 \times 10^{22}\ cm^{-3}\ s^{-1}$ for N_2:H_2 = 1:3 → 3:1) and Reaction 2 in the afterglows ($2.20 \times 10^{18} \rightarrow 3.94 \times 10^{17}\ cm^{-3}\ s^{-1}$ for N_2:H_2 = 1:3 → 3:1).

$$(\mathrm{md/ag})\quad \mathrm{N} + \mathrm{H_2}\left(\mathrm{b}^3\Sigma_u^+\right) \rightarrow \mathrm{H} + \mathrm{NH} \tag{R2}$$

$$(\mathrm{md/ag})\quad \mathrm{N} + \mathrm{H_2}\left(\mathrm{B}^1\Sigma_u^+\right) \rightarrow \mathrm{H} + \mathrm{NH} \tag{R3}$$

$$(\mathrm{md/ag})\quad \mathrm{N} + \mathrm{H_2}\left(\mathrm{c}^3\Pi_u\right) \rightarrow \mathrm{H} + \mathrm{NH} \tag{R4}$$

Moreover, the formation of NH(s) during a micro-discharge is largely a result of an ER reaction between ground state (X) or electrically excited (E) N and H(s) (Reaction 5, 96 % contribution) for the N_2-rich feed. Note that Reaction 5 is also the dominant path for the H_2-rich feed (80 % contribution of NH(s) formation in md), however, direct NH adsorption (Reaction 6) also contributes with 10 %, which is in contrast to the 3 % for the N_2-rich feed.

$$(\mathrm{md})\quad \mathrm{N(X,\ E)} + \mathrm{H(s)} \rightarrow \mathrm{NH(s)} \tag{R5}$$

$$(\mathrm{md})\quad \mathrm{NH} + \mathrm{surf} \rightarrow \mathrm{NH(s)} \tag{R6}$$

Similarly, during the micro-discharges, NH_2(s) is formed through an

ER route (Reaction 7) due to the high concentration of NH present in the short period (cf. Fig. 5c). Yet, for the N_2-rich feed, Reaction 8, a LH reaction, contributes with 9 % to the NH_2(s) formation, which for the H_2-rich feed only is 3 %. In the afterglows, Reaction 8 contributes with 99.6 % of the NH_2(s) formation for both feed ratios (N_2:H_2 = 3:1 and 1:3). The formed NH_2(s) is then solely used to form NH_3 through another LH reaction (Reaction 9) independently of feed ratio in both micro-discharges and afterglows. The feed ratio is therefore found to alter the contribution of the dominant reactions in the NH_3 synthesis mechanism and not to create/eliminate reaction steps.

$$(\mathrm{md})\quad \mathrm{NH} + \mathrm{H(s)} \rightarrow \mathrm{NH_2(s)} \tag{R7}$$

$$(\mathrm{md/ag})\quad \mathrm{NH(s)} + \mathrm{H(s)} \rightarrow \mathrm{NH_2(s)} + \mathrm{surf} \tag{R8}$$

$$(\mathrm{md/ag})\quad \mathrm{NH_2(s)} + \mathrm{H(s)} \rightarrow \mathrm{NH_3} + \mathrm{surf} + \mathrm{surf} \tag{R9}$$

Additionally, a net removal of NH_3 is predicted during micro-discharges (except for the very first micro-discharge), which is formed again in the afterglows, with the feed ratio only affecting the source terms slightly. For the feed ratio N_2:H_2 = 3:1, the source term in the micro-discharge is -1.14×10^{22} cm^{-3} s^{-1} and in the afterglow it is 3.95×10^{16} cm^{-3} s^{-1}, which changes to -1.09×10^{22} and 4.56×10^{16} cm^{-3} s^{-1} for N_2:H_2 = 1:3. This means that a lower rate of removal and higher rate of formation of NH_3 is observed for the H_2-rich feed, even though the NH_3 synthesis rate is higher for the N_2:H_2 = 3:1 feed ratio (cf. Fig. 4). However, to determine the amounts formed, the duration of a micro-discharge and the afterglow must be taken into account. In this study, the lifetime of a micro-discharge was determined to be 100 ns (see Table S1), while the duration of the afterglow was determined by the model to be 29.4 ms for N_2:H_2 = 3:1 and 23.6 ms for N_2:H_2 = 1:3. As a result of the longer afterglow the formation of NH_3 becomes higher for the N_2:H_2 = 3:1 feed ratio.

Interestingly, the formation of electrons in the micro-discharges is highest for the H_2-rich feed, which is not found to benefit the NH_3 synthesis (cf. Fig. 4). In contrast, the higher electron concentration leads to a higher NH_3 dissociation through Reaction 10 (3.92×10^{21} cm^{-3} s^{-1} for N_2:H_2 = 1:3 compared to 2.66×10^{21} cm^{-3} s^{-1} for N_2:H_2 = 3:1), while the dissociation through Reaction 11 is the same for both feed ratios (ca. 6.5×10^{21} cm^{-3} s^{-1}).

$$(\mathrm{md})\quad \mathrm{NH_3} + \mathrm{e^-} \rightarrow \mathrm{NH} + \mathrm{H_2} + \mathrm{e^-} \tag{R10}$$

$$(\mathrm{md})\quad \mathrm{NH_3} + \mathrm{e^-} \rightarrow \mathrm{NH_2} + \mathrm{H} + \mathrm{e^-} \tag{R11}$$

4.6. Experimental and modelled NH_3 concentration as function of residence time

A comparison of the model-predicted and the experimentally determined NH_3 concentration as function of the normalized residence time is presented in Fig. 9. As previously mentioned, the residence time was experimentally altered by changing the length of the outer electrode (1, 2, and 5 cm), thereby altering the plasma zone. The experimental residence times, at which the NH_3 concentrations were measured, were 1.2, 2.4, and 6.3 s for the unpacked setup (Exp-unpacked) and 0.4, 0.8, and 2.1 s for the packed setup (Exp-packed). However, on Fig. 9, normalized residence times are used for easier comparison. The Exp-packed results were obtained with $Co/MgAl_2O_4$.

From the model results, it can be observed that the unpacked case shows a continuously rising NH_3 concentration over the full residence time, with the destruction of NH_3 increasing during the micro-discharges at longer residence times, which indicates a gradual progress towards a cyclic steady state. Within the residence time of the unpacked case, a molecule is predicted to encounter 20 micro-discharges, which for the packed bed increases to 84 micro-discharges. In contrast to the unpacked reactor, the packed bed reactor quickly reaches a cyclic steady state, after encountering 15 micro-discharges, where the destruction of NH_3 in the micro-discharges equals the formation in the afterglows, as shown in Fig. 8. This is in agreement with the observations made by Navascués et al. [41] and Rouwenhorst et al. [45], who reported on the limiting effect of NH_3 decomposition, on the overall NH_3 concentration obtainable in the reactor outlet.

Similar to the simulated time-profile, the experimental results show an initial increase in NH_3 concentration with residence time (see Fig. 9), with a slower increase for the unpacked setup compared to the packed. For the packed system, the change in concentration is relatively limited for normalized residence times between 0.4 and 1, which is in reasonable agreement with the model. For the unpacked setup, an approximate steady state is also seen for a normalized residence time between 0.4 and 1, which is a contradiction to the gradually increasing production

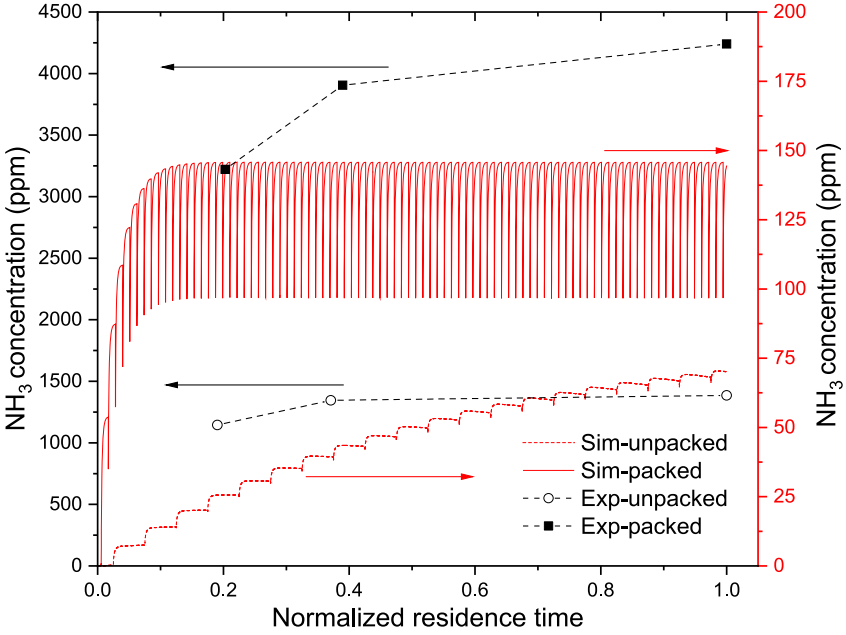

Fig. 9. NH_3 concentration as function of normalized residence time for unpacked and packed experiments and simulation. Full residence time for unpacked and packed reactor were 6 s and 2 s, respectively (feed flow rate of 80 Nml/min with a feed ratio of N_2:H_2 = 1:1 and plasma power of 15 W at 3.0 kHz).

predicted by the model. However, altering the length of the outer electrode also changes the electrical behavior of the setup (N_{MD}, τ_{MD}, Q_0, ΔU, C_{cell}, ζ_{diel}, C_{diel}), as reported in our previous work [9], hence additional simulations are needed for a true comparison between the model and experimental results. Since the model uses the electrical behavior of the experiment as input parameters, it is not capable of predicting the effects of the I, U, and Q parameters. To investigate the effects of these parameters, a 1D (or higher dimensional) model is needed, where the Poisson equation is solved, such that the electric field and current are calculated self consistently.

5. Conclusion

A combination of experiments and kinetic modeling was used to study the NH_3 synthesis from N_2 and H_2 in a DBD plasma reactor both without and with various packing materials. From experiments, it was found that increasing the feed flow rate improved the NH_3 synthesis rate for the tested packing materials and for the plasma alone. However, changing the gas temperature from 100 to 200 °C only enhanced the NH_3 synthesis rate when utilizing a packing material. For the packed setup, the model predicted a similar relative increase in NH_3 synthesis rate of 20 % when changing the temperature. At 200 °C an optimum in the NH_3 synthesis rate was observed with an equimolar feed ratio (N_2: H_2 = 1:1) for the plasma alone and $MgAl_2O_4$ packing, while a N_2-rich feed was favored for $Ru/MgAl_2O_4$ and $Co/MgAl_2O_4$ catalysts. Interestingly, a larger influence of the temperature was observed for the N_2-rich feed when packing material was utilized, while the plasma alone showed a slight decrease in the synthesis rate. This optimum in the synthesis rate with the N_2-rich feed, where high energy electrons are more likely to collide with N_2, suggests that the rate-limiting step is the dissociation of N_2 in the gas phase. The plasma kinetic model indicated a similar trend when packing material was used. However, for the plasma alone, the model found that the density of N in the gas phase does not affect the NH_3 synthesis rate when using a H_2-rich feed, whereas the limited access to hydrogen makes the hydrogenation of N species limiting in N_2-rich feeds.

The model predicted a cyclic steady state to be reached for the packed setup after encountering only 15 micro-discharges. This indicates that the catalytic NH_3 formation was not limited by the gas residence time at these conditions, but by the NH_3 dissociation rate in the micro-discharges. On the other hand, the plasma alone did not reach a steady state within the residence time of the gas and after encountering 20 micro-discharges.

A N_2-rich feed was found to yield a higher N density and a similar H (s) coverage compared to a H_2-rich feed, which in turn resulted in a higher coverage of NH(s) and NH_2(s). These surface species were revealed by the kinetic model to be formed through adsorption and elementary Eley-Rideal and Langmuir − Hinshelwood reactions, which therefore have a significant role in the plasma-catalytic NH_3 synthesis. Additionally, the feed ratio was found to modify the contribution of the dominant reaction steps leading to NH_3 formation and not to create new or eliminate existing reaction steps.

Declaration of Competing Interest

The authors declare that they have no known competing financial interests or personal relationships that could have appeared to influence the work reported in this paper.

Data availability

Data will be made available on request.

Acknowledgment

We thank Topsoe A/S for providing the catalytic materials used in the study, the research group PLASMANT (University of Antwerp) for sharing their plasma kinetic model and allocating time on their cluster for the calculations, and the Department of Chemical and Biochemical Engineering (Technical University of Denmark) for funding the project.

Appendix A. Supplementary data

Supplementary data to this article can be found online at https://doi.org/10.1016/j.cej.2023.141294.

References

[1] K.H.R. Rouwenhorst, L. Lefferts, Feasibility study of plasma-catalytic ammonia synthesis for energy storage applications, Catalysts 10 (2020) 999, https://doi.org/10.3390/catal10090999.
[2] A. Bogaerts, X. Tu, J.C. Whitehead, G. Centi, L. Lefferts, O. Guaitella, F. Azzolina-Jury, H.-H. Kim, A.B. Murphy, W.F. Schneider, T. Nozaki, J.C. Hicks, A. Rousseau, F. Thevenet, A. Khacef, M. Carreon, The 2020 plasma catalysis roadmap, J. Phys. D Appl. Phys. 53 (44) (2020) 443001.
[3] A. Bogaerts, E.C. Neyts, Plasma technology: an emerging technology for energy storage, ACS Energy Lett. 3 (2018) 1013–1027, https://doi.org/10.1021/acsenergylett.8b00184.
[4] J.A. Andersen, J.M. Christensen, M. Østberg, A. Bogaerts, A.D. Jensen, Plasma-catalytic dry reforming of methane: screening of catalytic materials in a coaxial packed-bed DBD reactor, Chem. Eng. J. (2020) 397, https://doi.org/10.1016/j.cej.2020.125519.
[5] I. Michielsen, Y. Uytdenhouwen, A. Bogaerts, V. Meynen, Altering conversion and product selectivity of dry reforming of methane in a dielectric barrier discharge by changing the dielectric packing material, Catalysts 9 (2019) 51, https://doi.org/10.3390/catal9010051.
[6] R. Snoeckx, A. Bogaerts, Plasma technology - a novel solution for CO_2 conversion? Chem. Soc. Rev. 46 (2017) 5805–5863, https://doi.org/10.1039/c6cs00066e.
[7] L. Wang, Y. Yi, C. Wu, H. Guo, X. Tu, One-step reforming of CO_2 and CH_4 into high-value liquid chemicals and fuels at room temperature by plasma-driven catalysis, Angew Chemie 56 (2017) 13679–13683, https://doi.org/10.1002/anie.201707131.
[8] J.A. Andersen, J.M. Christensen, M. Østberg, A. Bogaerts, A.D. Jensen, Plasma-catalytic ammonia decomposition using a packed-bed dielectric barrier discharge reactor, Int. J. Hydrogen Energy 47 (75) (2022) 32081–32091.
[9] Andersen JA, van 't Veer K, Christensen JM, Østberg M, Bogaerts A, Jensen AD. Ammonia decomposition in a dielectric barrier discharge plasma: Insights from experiments and kinetic modeling. Submitted 2022.
[10] M. Akiyama, K. Aihara, T. Sawaguchi, M. Matsukata, M. Iwamoto, Ammonia decomposition to clean hydrogen using non-thermal atmospheric-pressure plasma, Int. J. Hydrogen Energy 43 (2018) 14493–14497, https://doi.org/10.1016/j.ijhydene.2018.06.022.
[11] L. Wang, Y. Yi, Y. Zhao, R. Zhang, J. Zhang, H. Guo, NH_3 decomposition for H_2 generation: effects of cheap metals and supports on plasma-catalyst synergy, ACS Catal. 5 (2015) 4167–4174, https://doi.org/10.1021/acscatal.5b00728.
[12] M.L. Carreon, Plasma catalytic ammonia synthesis: state of the art and future directions, J. Phys. D Appl. Phys. 52 (48) (2019) 483001.
[13] N. Cherkasov, A.O. Ibhadon, P. Fitzpatrick, A review of the existing and alternative methods for greener nitrogen fixation, Chem. Eng. Process. 90 (2015) 24–33.
[14] P. Peng, P. Chen, C. Schiappacasse, N. Zhou, E. Anderson, D. Chen, J. Liu, Y. Cheng, R. Hatzenbeller, M. Addy, Y. Zhang, Y. Liu, R. Ruan, A review on the non-thermal plasma-assisted ammonia synthesis technologies, J. Clean. Prod. 177 (2018) 597–609.
[15] K.H.R. Rouwenhorst, Y. Engelmann, K. van 't Veer, R.S. Postma, A. Bogaerts, L. Lefferts, Plasma-driven catalysis: green ammonia synthesis with intermittent electricity, Green Chem. 22 (19) (2020) 6258–6287.
[16] K.H.R. Rouwenhorst, H.-H. Kim, L. Lefferts, Vibrationally excited activation of N_2 in plasma-enhanced catalytic ammonia synthesis: a kinetic analysis, ACS Sustain. Chem. Eng. 7 (2019) 17515–17522, https://doi.org/10.1021/acssuschemeng.9b04997.
[17] K.H.R. Rouwenhorst, H.G.B. Burbach, D.W. Vogel, J. Núñez Paulí, B. Geerdink, L. Lefferts, Plasma-catalytic ammonia synthesis beyond thermal equilibrium on Ru-based catalysts in non-thermal plasma, Cat. Sci. Technol. 11 (8) (2021) 2834–2843.
[18] Y. Engelmann, K. van 't Veer, Y. Gorbanev, E.C. Neyts, W.F. Schneider, A. Bogaerts, Plasma catalysis for ammonia synthesis: a microkinetic modeling study on the contributions of eley−rideal reactions, ACS Sustain. Chem. Eng. 9 (39) (2021) 13151–13163.
[19] Y. Gorbanev, Y. Engelmann, K. van't Veer, E. Vlasov, C. Ndayirinde, Y. Yi, S. Bals, A. Bogaerts, Al_2O_3-supported transition metals for plasma-catalytic NH_3 synthesis in a DBD plasma: metal activity and insights into mechanisms, Catalysts 11 (10) (2021) 1230.
[20] M. Iwamoto, M. Akiyama, K. Aihara, T. Deguchi, Ammonia synthesis on wool-like Au, Pt, Pd, Ag, or Cu electrode catalysts in nonthermal atmospheric-pressure plasma of N_2 and H_2, ACS Catal. 7 (2017) 6924–6929, https://doi.org/10.1021/acscatal.7b01624.
[21] P. Peng, Y. Cheng, R. Hatzenbeller, M. Addy, N. Zhou, C. Schiappacasse, D. Chen, Y. Zhang, E. Anderson, Y. Liu, P. Chen, R. Ruan, Ru-based multifunctional

mesoporous catalyst for low-pressure and non-thermal plasma synthesis of ammonia, Int. J. Hydrogen Energy 42 (30) (2017) 19056–19066.
[22] A. Gómez-Ramírez, J. Cotrino, R.M. Lambert, A.R. González-Elipe, Efficient synthesis of ammonia from N_2 and H_2 alone in a ferroelectric packed-bed DBD reactor, Plasma Sources Sci. Technol. 24 (2015), 065011, https://doi.org/10.1088/0963-0252/24/6/065011.
[23] M. Bai, Z. Zhang, X. Bai, M. Bai, W. Ning, Plasma synthesis of ammonia with a microgap dielectric barrier discharge at ambient pressure, IEEE Trans. Plasma Sci. 31 (2003) 1285–1291, https://doi.org/10.1109/TPS.2003.818761.
[24] X. Zhu, X. Hu, X. Wu, Y. Cai, H. Zhang, X. Tu, Ammonia synthesis over γ-Al_2O_3 pellets in a packed-bed dielectric barrier discharge reactor, J. Phys. D Appl. Phys. 53 (16) (2020) 164002.
[25] T. Riotto, G. Cao, W.L. Luyben, J. Baltrusaitis, Atmospheric pressure DBD plasma ammonia synthesis and separation process design and environmental impact assessment, ACS Sustain. Chem. Eng. 9 (2021) 13233–13244, https://doi.org/10.1021/acssuschemeng.1c04031.
[26] H.H. Kim, Y. Teramoto, A. Ogata, H. Takagi, T. Nanba, Atmospheric-pressure nonthermal plasma synthesis of ammonia over ruthenium catalysts, Plasma Process Polym 14 (2017) e201600157.
[27] F. Gorky, S.R. Guthrie, C.S. Smoljan, J.M. Crawford, M.A. Carreon, M.L. Carreon, Plasma ammonia synthesis over mesoporous silica SBA-15, J. Phys. D Appl. Phys. 54 (26) (2021) 264003.
[28] F. Gorky, A. Best, J. Jasinski, B.J. Allen, A.C. Alba-Rubio, M.L. Carreon, Plasma catalytic ammonia synthesis on Ni nanoparticles: the size effect, J. Catal. 393 (2021) 369–380, https://doi.org/10.1016/j.jcat.2020.11.030.
[29] E.C. Neyts, Plasma-surface interactions in plasma catalysis, Plasma Chem. Plasma Process. 36 (2016) 185–212, https://doi.org/10.1007/s11090-015-9662-5.
[30] P. Mehta, P. Barboun, F.A. Herrera, J. Kim, P. Rumbach, D.B. Go, J.C. Hicks, W. F. Schneider, Overcoming ammonia synthesis scaling relations with plasma-enabled catalysis, Nat. Catal. 1 (4) (2018) 269–275.
[31] J. Hong, S. Pancheshnyi, E. Tam, J.J. Lowke, S. Prawer, A.B. Murphy, Kinetic modelling of NH_3 production in N_2–H_2 non-equilibrium atmospheric-pressure plasma catalysis, J. Phys. D Appl. Phys. 50 (2017), 154005, https://doi.org/10.1088/1361-6463/aaa988.
[32] K. van 't Veer, Y. Engelmann, F. Reniers, A. Bogaerts, Plasma-catalytic ammonia synthesis in a DBD Plasma: role of microdischarges and their afterglows, J. Phys. Chem. C 124 (42) (2020) 22871–22883.
[33] Pancheshnyi S, Eismann B, Hagelaar GJM, Pitchford LC. Computer code ZDPlasKin 2008:University of Toulouse, LAPLACE, CNRS-UPS-INP, Fra. http://www.zdplaskin.laplace.univ-tlse.fr/.
[34] G.J.M. Hagelaar, L.C. Pitchford, Solving the Boltzmann equation to obtain electron transport coefficients and rate coefficients for fluid models, Plasma Sources Sci. Technol. 14 (2005) 722–733, https://doi.org/10.1088/0963-0252/14/4/011.
[35] K. van 't Veer, F. Reniers, A. Bogaerts, Zero-dimensional modelling of unpacked and packed bed dielectric barrier discharges: The role of vibrational kinetics in ammonia synthesis, Plasma Sources Sci. Technol. 29 (2020) 45020, https://doi.org/10.1088/1361-6595/ab7a8a.
[36] Q.-Z. Zhang, W.-Z. Wang, A. Bogaerts, Importance of surface charging during plasma streamer propagation in catalyst pores, Plasma Sources Sci. Technol. 27 (6) (2018) 065009.
[37] Q.-Z. Zhang, A. Bogaerts, Propagation of a plasma streamer in catalyst pores, Plasma Sources Sci. Technol. 27 (2018), 035009, https://doi.org/10.1088/1361-6595/aab47a.
[38] R.D. Cortright, J.A. Dumesic, Kinetics of heterogeneous catalytic reactions: analysis of reaction schemes, Adv. Catal. 46 (2001) 161–264.
[39] A. Bogaerts, W. Wang, A. Berthelot, V. Guerra, Modeling plasma-based CO_2 conversion: crucial role of the dissociation cross section, Plasma Sources Sci. Technol. 25 (2016), 055016, https://doi.org/10.1088/0963-0252/25/5/055016.
[40] J. Hong, S. Prawer, A.B. Murphy, Plasma catalysis as an alternative route for ammonia production: status, mechanisms, and prospects for progress, ACS Sustain. Chem. Eng. 6 (2018) 15–31, https://doi.org/10.1021/acssuschemeng.7b02381.
[41] P.N. Navascués, J.M. Obrero-Pérez, J. Cotrino, A.R. González-Elipe, A. Gómez-Ramírez, Unraveling discharge and surface mechanisms in plasma-assisted ammonia reactions, ACS Sustain. Chem. Eng. 8 (2020) 14855–14866, https://doi.org/10.1021/acssuschemeng.0c04461.
[42] C. Stegelmann, A. Andreasen, C.T. Campbell, Degree of rate control: how much the energies of intermediates and transition states control rates, J. Am. Chem. Soc. 131 (2009) 8077–8082, https://doi.org/10.1021/ja9000097.
[43] L.R. Winter, B. Ashford, J. Hong, A.B. Murphy, J.G. Chen, Identifying surface reaction intermediates in plasma catalytic ammonia synthesis, ACS Catal. 10 (2020) 14763–14774, https://doi.org/10.1021/acscatal.0c03166.
[44] J. Shah, F. Gorky, P. Psarras, B. Seong, D.A. Gómez-Gualdrón, M.L. Carreon, Enhancement of the yield of ammonia by hydrogen-sink effect during plasma catalysis, ChemCatChem 12 (2020) 1200–1211, https://doi.org/10.1002/CCTC.201901769.
[45] K.H.R. Rouwenhorst, S. Mani, L. Lefferts, Improving the energy yield of plasma-based ammonia synthesis with in situ adsorption, ACS Sustain. Chem. Eng. 10 (2022) 1994–2000, https://doi.org/10.1021/acssuschemeng.1c08467.